Progress in Photovoltaics: Research and Applications

WILEY

PROGRESS IN PHOTOVOLTAICS

RESEARCH ARTICLE OPEN ACCESS

Higher-Efficiency TOPCon Solar Cells in Mass Production Enabled by Laser-Assisted Firing: Advanced Loss Analysis and Near-Term Efficiency Potential

Xutao Wang[1] | Jing Yuan[2] | Xinyuan Wu[1] | Jianjun Nie[2] | Yanyan Zhang[2] | Xiaoyan Zhang[2] | Weiguang Yang[2] | Feng Li[2] | Bram Hoex[1]

[1]School of Photovoltaic and Renewable Energy Engineering, University of New South Wales, Sydney, Australia | [2]Jolywood (Taizhou) Solar Technology Co., Ltd, Taizhou, Jiangsu, China

Correspondence: Xutao Wang (xutao.wang@unsw.edu.au) | Xinyuan Wu (xinyuan.wu@unsw.edu.au) | Feng Li (boven@jolywood.cn) | Bram Hoex (b.hoex@unsw.edu.au)

Received: 25 August 2024 | **Revised:** 30 March 2025 | **Accepted:** 22 April 2025

Funding: This work was supported by Australian Renewable Energy Agency, Australian Government's Trailblazer for Recycling & Clean Energy program, Australian Centre for Advanced Photovoltaics (ACAP).

Keywords: high-volume production | laser-assisted firing | loss analysis | metal contact recombination | metallization | TOPCon solar cell

ABSTRACT

The tunnel oxide passivated contact (TOPCon) solar cell is predicted to dominate the photovoltaic market from the year 2024. The TOPCon efficiency is steadily increasing both in the lab and high-volume production. A notable new manufacturing technology, laser-assisted firing, has been shown to enhance the power conversion efficiency (*PCE*) of TOPCon solar cells. This enhanced contact firing technique includes a traditional co-firing step, followed by a laser scanning process in conjunction with an applied reverse bias. In this work, we utilize the Jolywood Special Injected Metallization (JSIM), a laser-assisted firing process developed by Jolywood that is already used in high-volume production. The performance of cells from the JSIM process was evaluated by comparing them to the cells fabricated using the baseline (BL) single-step firing process. The JSIM solar cells exhibited a notably higher *PCE*, approximately 0.58%$_{abs}$ greater, compared with the BL cells. Detailed characterization demonstrated that the front (~280 fA/cm^2) and rear (~98 fA/cm^2) contact recombination of baseline (BL) cells are higher than those of JSIM cells (~88 fA/cm^2 and ~21 fA/cm^2, respectively), which is also the main advantages of the JSIM technology. Quokka 3 simulations were utilized to quantify the impact of the various improvements on the final solar cell performance. With the utilization of JSIM technology, contact recombination is no longer the primary source of power loss across the cell. Finally, the simulated results illustrated that the *PCE* of industrial JSIM cells could further be enhanced by ~0.3%$_{abs}$ through optimizing the front screen pattern. This work clearly demonstrates the feasibility of laser-assisted firing in high-volume production, enabling significantly higher efficiency TOPCon solar cells by significantly reducing silicon-metal recombination. Consequently, laser-assisted firing increases the practical efficiency limit of TOPCon solar cells, bringing them close to levels that were previously only envisioned for heterojunction silicon solar cells.

1 | Introduction

Photovoltaic (PV) manufacturers are continually striving to boost the power conversion efficiency (*PCE*) of solar cells. As one of the leading technologies, the tunnel oxide passivated contact (TOPCon) solar technology [1–6] is considered capable of approaching the efficiency limit of single-junction silicon solar cells. Certified *PCE* values of up to 26.58% have been reported

for industrial-sized TOPCon solar cells [7, 8]. Due to its performance and high compatibility with the passivated emitter and rear contact (PERC) cell production lines [9], the TOPCon solar cell has become the dominant technology in the PV market from 2024 [10] with a significant focus on improving its performance [11–17].

Recently, laser-assisted firing technology [18–22] has gained considerable interest as an advanced method for improving the firing process in silicon solar cell production. The best-known example of laser-assisted firing is the laser-enhanced contact optimization (LECO) technology [23, 24]. The LECO technology was initially invented to recover cells with poor ohmic-contact behavior caused by faulty firing process control [25], but was then found to be able to effectively enhance the efficiency of PERC solar cells [22, 26, 27]. Mayberry et al. [28] demonstrated the positive effect of LECO on the power output of solar cells. With the application of laser-assisted firing and customized paste, the p-type PERC cells with homogenous emitter showed ~0.14%$_{abs}$ increase in *PCE* compared with control cells with standard paste and firing process. Höffler et al. [27] also utilized a laser to scan the whole area of cells to locally generate charge carriers and thus formed the metal-Si contact by the induced high density of local current. It was reported that the firing window of PERC cells with standard silver (Ag) screen printing paste could be enlarged. With the utilization of customized paste, the cell efficiency could even be ~0.37%$_{abs}$ higher. Moreover, the metal-Si contact of PERC cells under laser-assisted firing was found to be located at or near the peaks of pyramids. Based on the unique contact structure, the current-fired contact (CFC) theory [29] was developed and illustrated that part of the passivation layer between metal and Si could be preserved during the firing process and thus potentially lead to lower recombination loss caused by a reduced metal-Si formation. Based on the promising results on PERC solar cells, researchers started to test the potential of laser-assisted firing on TOPCon solar cells. Fellmeth et al. [21] applied low-temperature firing together with a laser-assisted firing process to TOPCon solar cells and presented ~0.6%$_{abs}$ *PCE* gain, compared with standard cells fabricated using an optimized single-step co-firing process. The effect of some key parameters during the process, including reverse bias, laser intensity, current density, etc., on the optimization of cell performance was investigated by Xie et al. [30] to illustrate their influencing mechanisms. Fan et al. [31] further extended the efficiency improvement results to propose a new physical model, illustrating that for TOPCon solar cells under laser-assisted firing, metal-Si contacts mainly formed on the top of the pyramid, while Ag colloids and glass frit were found at the bottom of the pyramid. Moreover, Wang et al. [32] and Zhou et al. [33] analyzed the metal-Si contact structure using transmission electron microscopy (TEM) technology, demonstrating that the Ag–Si eutectic alloy structure as well as high Ag-content glass layer with better glass passivation performance and improved conductivity, contribute to the efficiency enhancement of cells based on the laser-assisted firing technology. Furthermore, our recent work [34] demonstrated that the laser-assisted firing technology not only increases the cell efficiency but also significantly enhances the corrosion resistance of TOPCon solar cells. Similar to our results, Mette et al. [35] presented improved efficiency as well as low degradation under thermal cycling and damp-heat testings on Qcells' Q.ANTUM NEO solar devices, with the utilization of LECO technology.

While laser-assisted firing on TOPCon solar cells has garnered increasing attention, most research remains confined to the laboratory level instead of high-volume production. Additionally, loss analysis of cells subjected to laser-assisted firing is still scarce, with many electrical factors yet to be thoroughly quantified and discussed. In this work, we focus on a laser-assisted firing process, the Jolywood Special Injected Metallization (JSIM) [34] developed by Jolywood, which is already utilized in high-volume production and compare its performance to the baseline single-step co-firing process. To compare the optimized performance of both technologies, state-of-the-art cells from the high-volume production of each technology were taken. The experimental results demonstrated that JSIM cells with homogenous emitter (HE) had superior performance to baseline cells with selective emitter (SE), presenting ~0.58%$_{abs}$ higher *PCE* and an ~11.7 mV higher V_{oc}. The detailed characterization data showed that JSIM cells benefited from lower front and rear contact recombination but suffered from higher front contact resistivity due to the lack of selective emitter. To quantify the difference between the two technologies, Quokka 3 [36] simulations were conducted. The loss analysis emphasized the superiority of JSIM technology in reducing contact recombination, which contributed to the most significant power loss in baseline cells. Finally, the simulated results indicated that the *PCE* of JSIM cells could be further improved by ~0.3%$_{abs}$ with just the optimization of front grid pattern design, leaving additional room for improvement when combined with other process optimization steps.

2 | Methodology

In this work, we compared the performance of state-of-the-art baseline (BL) TOPCon cells with newly designed TOPCon cells fabricated using JSIM process. Both technologies are used in high-volume industrial production, and the process flow is shown in Figure 1a. M10 (182.2 × 183.75 mm) n-type Si substrates with a thickness of 130 μm and a resistivity of 1 Ω·cm were used. All wafers underwent cleaning and texturing to create pyramid structures on the surface. Next, boron diffusion fabricated the front-side p^+ emitter. For the BL cells, a laser doping process was then employed to form localized p^{++} regions on the front (i.e., a selective emitter [SE]), as shown in Figure 1c. Therefore, the JSIM cell used a homogenous emitter (HE) structure while the BL cell featured a selective emitter (SE). After that, the borosilicate glass (BSG) layer was removed and the rear side was polished through acid etching and alkaline polishing processes. A tunneling SiO_x layer and a poly-Si layer were then formed on the back using plasma oxidation and plasma-assisted in situ doping deposition (POPAID), followed by a buffered oxide etch (BOE) cleaning process. The surface passivation layers were atomic layer deposited (ALD) AlO_x and plasma-enhanced chemical vapor deposition (PECVD) SiN_x layers on the front side, as well as a PECVD SiN_x passivation layer on the rear side. For the baseline (BL) group, cells were produced using a traditional metallization process with commercial Al/Ag front screen printing paste and a traditional single-step industrial firing process. In

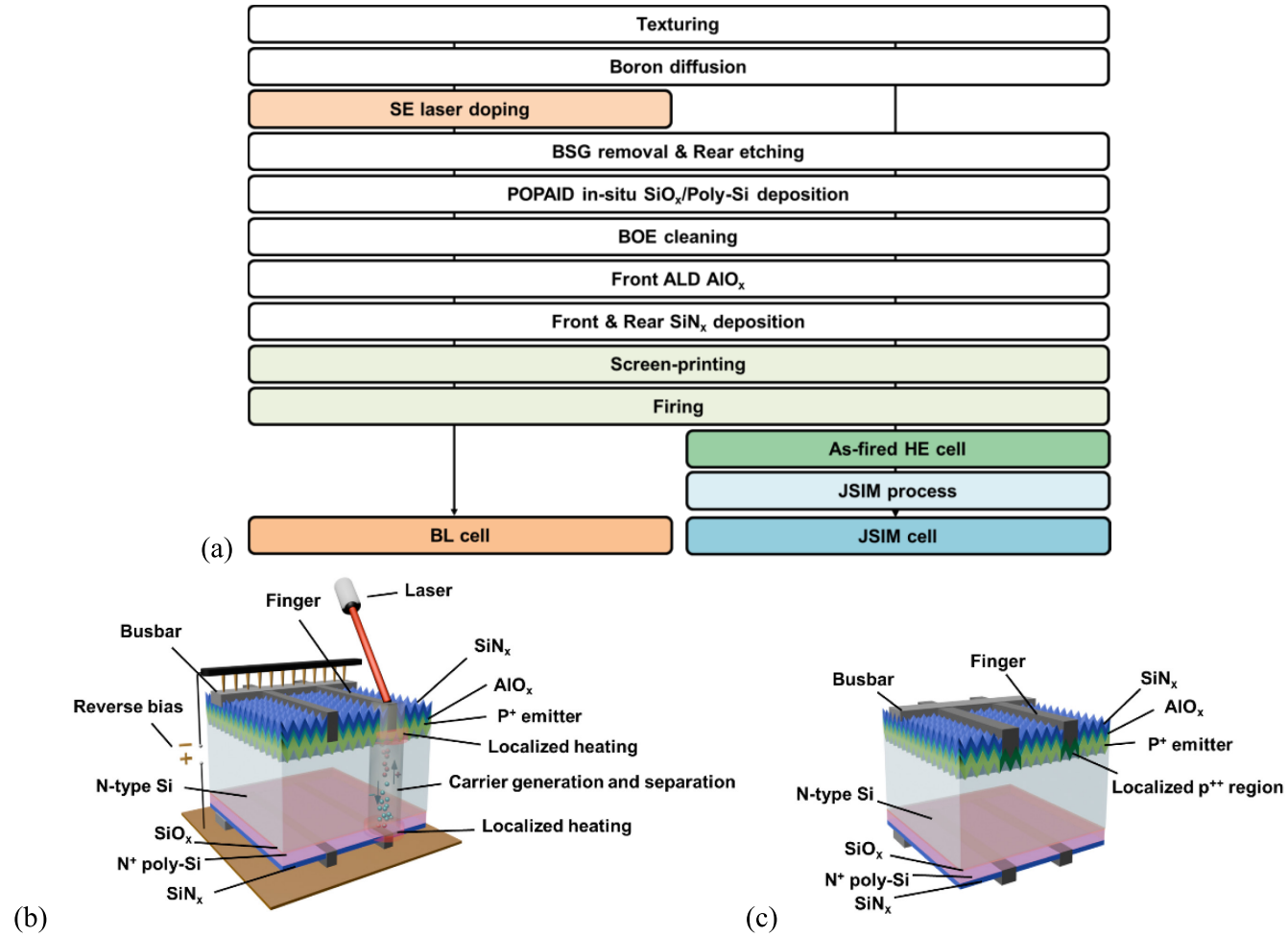

FIGURE 1 | (a) Process flowchart of BL, as fired HE and JSIM cells, schematic of (b) the homogenous TOPCon solar cell with JSIM process and (c) baseline TOPCon solar cell used in this work.

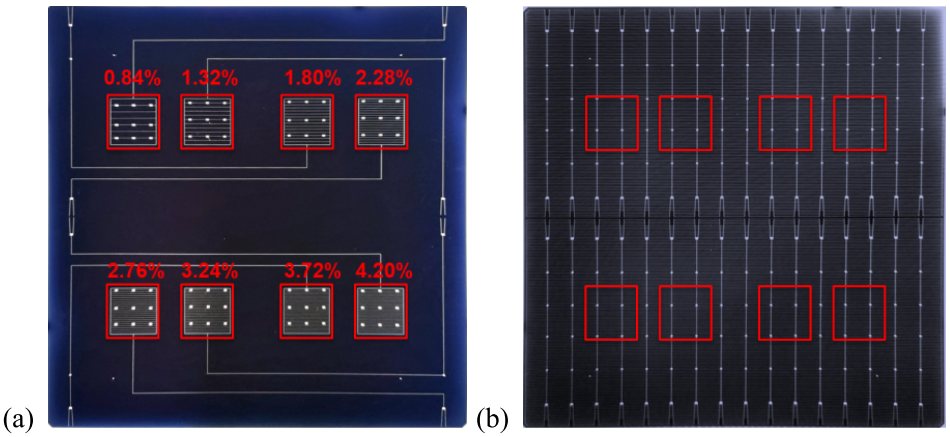

FIGURE 2 | (a) Special sub-cell design with various contact area fractions for the front side and (b) rear-side grids with the same corresponding rear pattern for each sub-cell.

comparison, the JSIM samples utilized a specialized Ag front finger paste and underwent firing at a temperature about 30 °C lower, followed by the JSIM process, which incorporates a laser line scanning procedure combined with an applied reverse bias (schematically shown in Figure 1b). The laser, with a wavelength of 1064 nm and a frequency of 50 kHz, scans the fingers and the regions near them, locally generating charge carriers that are separated by the applied reverse bias voltage of 17.5 V. The current flows through the areas with a relatively low contact resistance between silicon and metal, which results in localized heating at the metal-Si contact, significantly reducing the contact resistance in these areas while leaving the non-contacted areas unaffected [37]. Notably, both BL and JSIM cells have the same screen-printing pattern design.

The metal-induced recombination of samples was obtained by combining experimental Suns-V_{oc} measurement with Quokka 3 simulations to take into account the lateral balancing current [38–40]. Figure 2 shows the specially designed samples used to extract metal-induced recombination of both the BL and JSIM samples. Eight sub-cells were fabricated on the front side of samples. As shown in Figure 2a, the metal contact fraction was varied by changing the finger pitch from 2.86 to 0.57 mm. Each sub-cell was adequately separated to minimize interference. For the rear side in Figure 2b, a normal pattern design for cells was utilized. Importantly, the positions of sub-cells were carefully selected to ensure each of them had the same corresponding rear pattern, allowing the same rear grid design to be modeled for each sub-cell in the following simulation. Suns-V_{oc} measurements were performed on each sub-cell using a Sinton Instruments WCT-120 Suns-V_{oc} tester. Referring to the experimental/simulation flowchart shown in Figure 3, the rear side passivated recombination density ($J_{0,rear\text{-}pas}$) and bulk lifetime (τ_{bulk}) information were extracted from as-fired double-side poly-Si wafers passivated by PECVD SiN_x. The front side full area passivated recombination ($J_{0,front\text{-}pas}$) was adjusted to meet the measured implied open-circuit voltage ($iV_{oc,HE}$) of fired HE precursors. Based on the previous parameters, the localized passivated recombination density ($J_{0,local\ front\text{-}pas}$) at SE regions for BL samples was modified according to the implied open-circuit voltage ($iV_{oc,SE}$) of SE precursors after firing. All lifetime measurements were completed on a Sinton Instruments WCT-120 lifetime tester. After recreating the models, the front finger pitch was swept based on the special pattern design, and both the front ($J_{0,front\text{-}met}$) and rear contact recombination ($J_{0,rear\text{-}met}$) were optimized together to fit the simulated V_{oc} with the measured 1-sun V_{oc} of each sub-cell. In addition, an ASICCN SCSS electroluminescence (EL) tool was used to capture the EL images of cells. A ZEISS Cryogenic focused ion beam (Cryo-FIB)-SEM tool was used to cut through the finger contact of the cells, and the energy dispersive spectroscopy (EDS) data was measured by the Oxford Instruments Ultim® Max and analyzed with AZtec software. The one-sun current–voltage (I-V) parameters of cells were measured by a Sinton Instruments FCT650 I-V tester (employing an Xe flash). A PV-Tools TLM-SCAN+ tool was employed to perform the transfer length method (TLM) measurement to determine the contact resistivity between silicon and the metal. Additionally, the line resistance of the solar cells was measured on a four-point probe station.

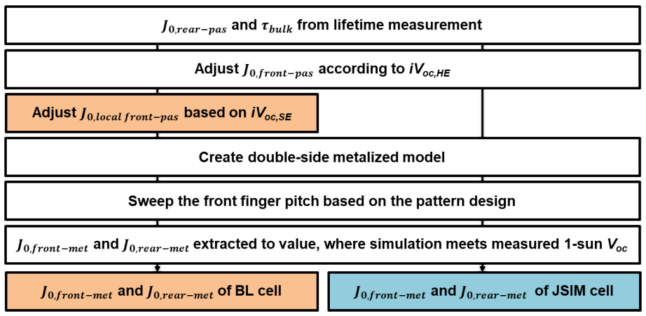

FIGURE 3 | Schematic flow for the simulation-based evaluation of double-side contact recombination using Quokka 3.

3 | Results and Discussion

3.1 | EL Images of JSIM Cells and Paste Analysis

Figure 4 shows the EL images of the as-fired HE cell as well as the HE cell after the JSIM process, illustrated in Figure 1a. In Figure 4a, the EL image reveals poor electrical contact in the solar cell after the low-temperature firing process. In contrast, after the JSIM process, the EL image shown in Figure 1b presents relatively more uniform and better electrical performance. This result is consistent with the previously reported work [31], indicating that the JSIM process is essential for providing a localized high temperature to form a reliable metal-Si contact.

To investigate the poor contact of as-fired samples, cross-sectional EDS analysis was applied to the front metal contact of JSIM and BL samples to study the difference between front metal pastes. As expected, Figure 5 illustrates that both metal contacts predominantly contained Ag. However, the BL samples showed a clear presence of Al in the contacts, whereas negligible Al signal could be detected in the JSIM metal contacts. Moreover, Table 1 presents the detailed weight ratio of Al and Pb to Ag for the corresponding cross-sectional BL and JSIM front contact. According to the EDS elemental results, the weight ratio of both Pb and Al of JSIM paste was much lower than BL paste, indicating that JSIM cells used a customized paste with a lower concentration of glass frit and Al

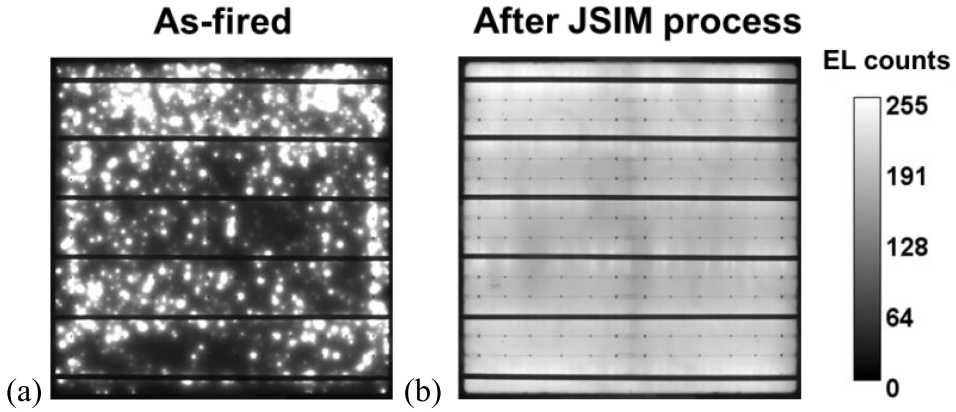

FIGURE 4 | EL images of (a) the as-fired HE cell and (b) the HE cell after JSIM process illustrated in Figure 1a.

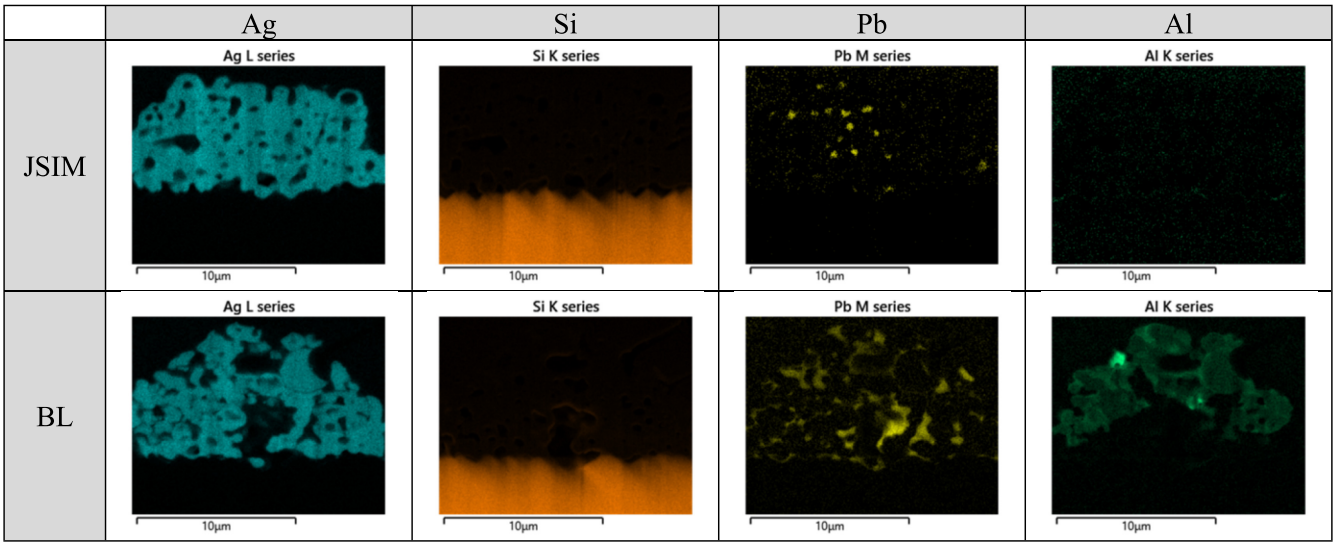

FIGURE 5 | Cross-sectional EDS mappings for Ag, Si, Pb, and Al of front metal contact of JSIM and BL samples.

TABLE 1 | The EDS elemental weight ratio of Al and Pb to Ag within JSIM and BL cross-sectional samples in Figure 5.

	Weight ratio (Pb/Ag)	Weight ratio (Al/Ag)
JSIM paste	0.9%	0.1%
BL paste	5.3%	2.5%

additives. Considering that both components are crucial for the metal paste to penetrate through the passivation layer to contact Si [41–44], the difference in Pb and Al concentration, in combination with the slightly lower firing temperature, explains the relatively poor contact in the JSIM group prior to the laser-assisted firing step. However, the difference in paste composition and lower firing temperature may also result in a lower metal-induced recombination, which could enable higher V_{oc} values.

3.2 | I-V Results

Figure 6 shows and compares the I-V parameters of as-fired HE, JSIM and BL cells. The average power conversion efficiency (*PCE*) of the as-fired HE cells was only ~0.01%. This poor performance was mainly affected by the significantly low fill factor (*FF*) and short-circuit current (J_{sc}), which could be attributed to poor contact and carrier collection ability, as shown in Figure 4a. The *PCE* of JSIM cells was 25.08%, surpassing the BL cells with an average value of 24.50%. Regarding the detailed differences, JSIM cells showed slightly higher J_{sc} than BL cells. Considering both cells used the same screen-printing pattern, the variation could likely be attributed to the parasitic blue light absorption of SE regions [45–47], which have much lower localized sheet resistance and, thus, higher dopant concentration. In addition, the main divergence between the two groups of cells was the V_{oc}, where JSIM cells had an average of 733.8 mV, much higher than the 722.1 mV average value of the BL cells. Interestingly, the average *FF* of JSIM and BL cells were quite similar, with only ~0.1% absolute difference. Except for the $J_{sc,}$ which was mainly dominated by light absorption, both V_{oc} and *FF* involved complex effects induced by multiple factors. Therefore, the performance differences between JSIM and BL cells warrant further discussion.

3.3 | Contact Resistivity and Line Resistance

Due to the use of different front paste and metallization/firing technology, the detailed characterization discussion first focused on the contact resistivity and line resistance differences between JSIM and BL cells. In Figure 7a, no significant difference could be observed in the rear contact resistivity of JSIM and BL cells, indicating that those two firing technologies did not affect the rear contact carrier transport. However, the JSIM cells showed higher contact resistivity at the front side compared with BL cells. Interestingly, the laser-assisted firing process was reported to be able to reduce the front contact resistivity compared with baseline firing [21, 31]. As a result, the lower front contact resistivity of BL cells in this study is likely due to the presence of SE regions, which can effectively lower the contact resistivity compared with the lightly doped emitter, in addition to the lower silicon-metal contact fraction for the JSIM group. The measured line resistance of JSIM and BL cells is presented in Figure 7b. Similar to the results of contact resistivity, the rear side of both cells had consistent line resistance, which can be attributed to the same pattern design and paste. In contrast, the front-side line resistance of JSIM cells was relatively lower than that of BL cells, owing to the customized paste with a lower concentration of glass frit and Al additives.

3.4 | Variation of Parasitic Recombination Loss

To gain a deeper understanding of the parasitic recombination loss caused by different processes, HE and SE precursors were utilized for implied open circuit voltage (iV_{oc}) measurement. Figure 8 shows the measured iV_{oc} of precursors after different firing processes. HE-JSIM refers to HE precursors

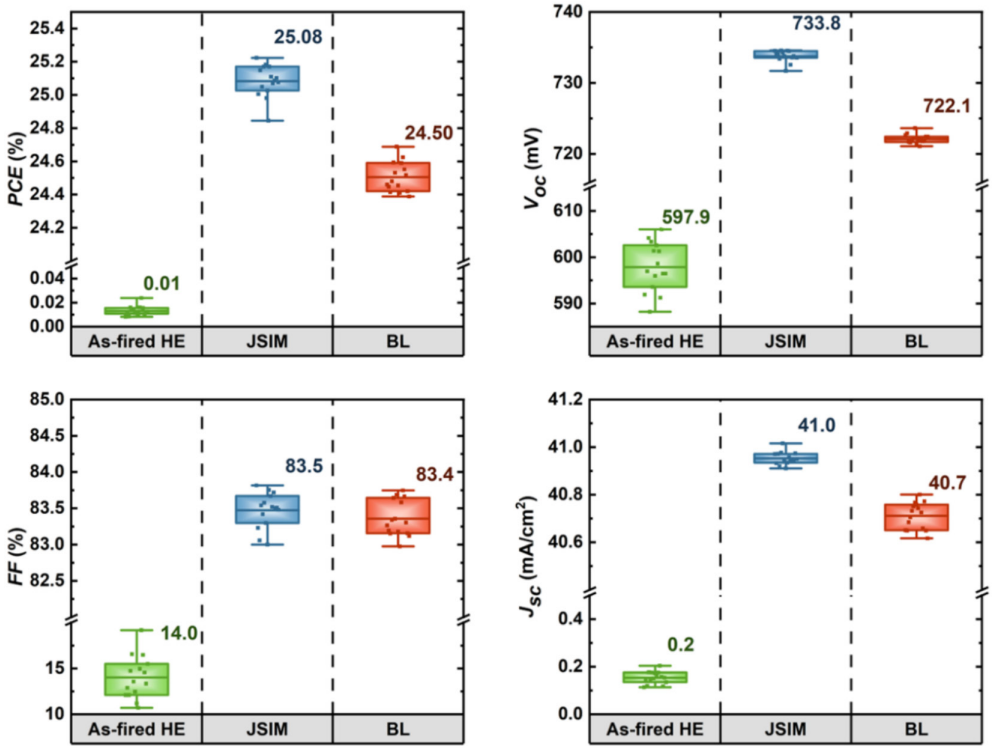

FIGURE 6 | One-sun *PCE*, V_{oc}, *FF*, and J_{sc} values of as-fired HE, JSIM, and BL cells illustrated in Figure 1a.

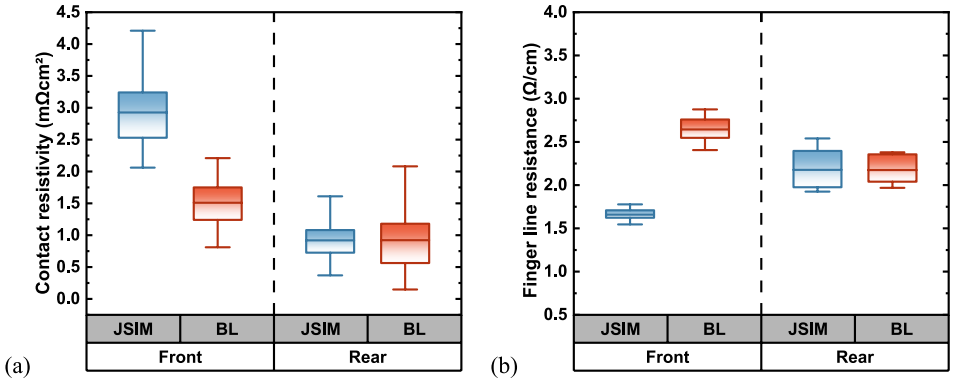

FIGURE 7 | Front and rear (a) contact resistivity and (b) line resistance of JSIM and BL cells.

that underwent a JSIM cell low-temperature firing process. HE-BL and SE-BL represent HE and SE precursors that underwent a baseline firing. Therefore, HE-JSIM and SE-BL could indicate the performance of fired precursors of JSIM and BL groups, respectively, and the HE-BL was a reference group. As shown in Figure 8, HE-JSIM and HE-BL showed a consistent iV_{oc}, illustrating that the variation of the firing temperature did not materially affect the bulk and surface passivation on the front and the rear of the solar cell. However, compared with HE-JSIM, the iV_{oc} of SE-BL precursors was relatively lower. As the effect of firing temperature has been excluded, the iV_{oc} difference could be attributed to the SE laser doping process [48–50]. In addition, it is worth mentioning that the iV_{oc} gap between JSIM and BL precursors was still lower than the V_{oc} deviation of JSIM and BL cells, as shown in Figure 6. Therefore, the metal-induced recombination of JSIM cells was found to be lower than BL cells.

Then, the metal-induced recombination of both groups of cells was quantified. Figure 9 shows the measured and simulated V_{oc} of sub-cells with different front contact fractions. For both JSIM and BL samples, the contact fraction and the V_{oc} showed an approximate linear relation. The fitted $J_{0,front\text{-}met}$ of JSIM cells (~88 fA/cm^2) was found to be lower than that of BL cells (~280 fA/cm^2). The rear metal-induced recombination $J_{0,rear\text{-}met}$ was quantified to be ~21 fA/cm^2 for the JSIM cells and ~98 fA/cm^2 for BL cells. The extracted front and rear contact recombination of BL cells were close to the values reported previously [51–53]. Moreover, a similar reduction of rear contact recombination for TOPCon solar cells was observed when the researchers decreased the peak firing temperature from 840 to 800°C [21]. Therefore, the lower rear contact recombination of the JSIM cell might be attributed to its lower firing temperature. In conclusion, the JSIM cells were proven to perform lower metal-induced recombination for both the front and rear sides.

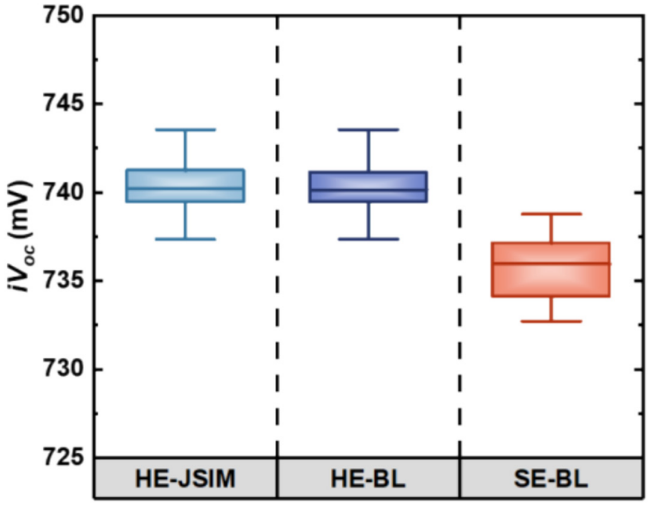

FIGURE 8 | Measured iV_{oc} of HE and SE precursors after the corresponding firing process.

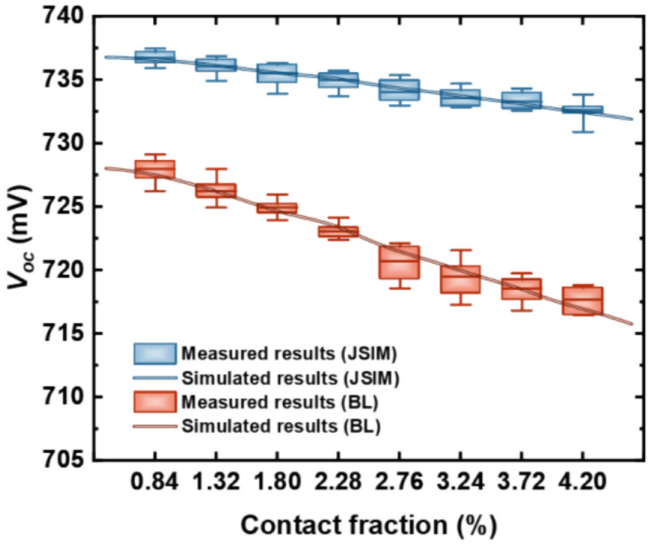

FIGURE 9 | Measured and simulated V_{oc} of sub-cells with different front contact fractions for the evaluation of front and rear metal-induced recombination of JSIM and BL cells.

3.5 | Quokka 3 Simulation Results

3.5.1 | JSIM and BL Performance Comparison

The simulated performance parameters presented in Table 2 align well with the measured parameters obtained from the light I-V measurements. The consistent simulated results further proved the reliability of the recreated simulation model for both BL and JSIM cells, enabling the performance comparison between those two groups of cells through simulation.

As mentioned in Section 3.2, in this study, both V_{oc} and *FF* were affected by complex interactions of multiple factors. Therefore, the simulated V_{oc}, *FF*, and *PCE* comparison between BL and JSIM cells is shown in Figure 10 in the form of a waterfall diagram. Based on the simulated results, the primary improvement of JSIM cells was the decrease of front and rear contact recombination. As shown in Figure 10, the lower contact recombination provided ~9.37 mV increase of V_{oc} and ~0.36%$_{abs}$ enhancement of *FF*, which resulted in ~0.42%$_{abs}$ higher *PCE*. The V_{oc} of JSIM cells was also improved by the absence of the SE. However, the lower overall conductance of the homogeneous emitter resulted in a ~0.04% lower *FF*. Nevertheless, combined with the benefits from lower recombination loss, the *PCE* still showed ~0.07%$_{abs}$ enhancement. Additionally, the relatively higher front contact resistivity decreased the *FF* by ~0.32%$_{abs}$ for the JSIM cells. Despite the *FF* loss, the overall *FF* of JSIM cells is still higher than the baseline due to the gain from lower recombination as well as lower front line resistance. For the *PCE*, almost all factors showed positive effects on JSIM cells except for higher contact resistivity. Therefore, the overall simulated *PCE* of JSIM was ~0.61%$_{abs}$ higher than BL cells.

TABLE 2 | The comparison between average measured and simulated V_{oc}, J_{sc}, *FF*, and *PCE* of both JSIM and BL cells.

		V_{oc} (mV)	J_{sc} (mA/cm^2)	*FF* (%)	*PCE* (%)
JSIM	Average measured results	733.8	41.0	83.5	25.1
	Simulated results	734.7	41.0	83.7	25.2
BL	Average measured results	722.1	40.7	83.4	24.5
	Simulated results	722.5	40.7	83.6	24.6

3.5.2 | Electrical Loss Analysis and Potential for Improvement

The electrical losses of BL and JSIM cells were analyzed using the free energy loss analysis method (FELA) implemented in Quokka 3 [54]. The loss breakdown, including recombination and resistive losses, is shown in Figure 11. Figure 11a shows the loss analysis of BL cells, which suffered the most from recombination at the front and rear contact, with power losses of ~0.26 mW/cm^2 and ~0.20 mW/cm^2, respectively. Another main contributor was the front hole transport loss (~0.19 mW/cm^2), which was primarily related to the lateral transport in the high-sheet resistance emitter. In addition, the bulk region also presented certain losses due to intrinsic and extrinsic recombination, showing a total ~0.32 mW/cm^2 recombination-induced power loss. Figure 11b shows the loss breakdown of JSIM cells, which can also provide directions to improve the cell performance further. In contrast to the BL cells, the power loss of JSIM cells due to front (~0.14 mW/cm^2) and rear contact recombination (~0.08 mW/cm^2) were significantly reduced and no longer dominated the overall power loss. By contrast, the bulk intrinsic recombination in JSIM cells presented the most contribution with a loss of ~0.35 mW/cm^2. The results indicate that utilizing Si bulk with higher resistivity might be

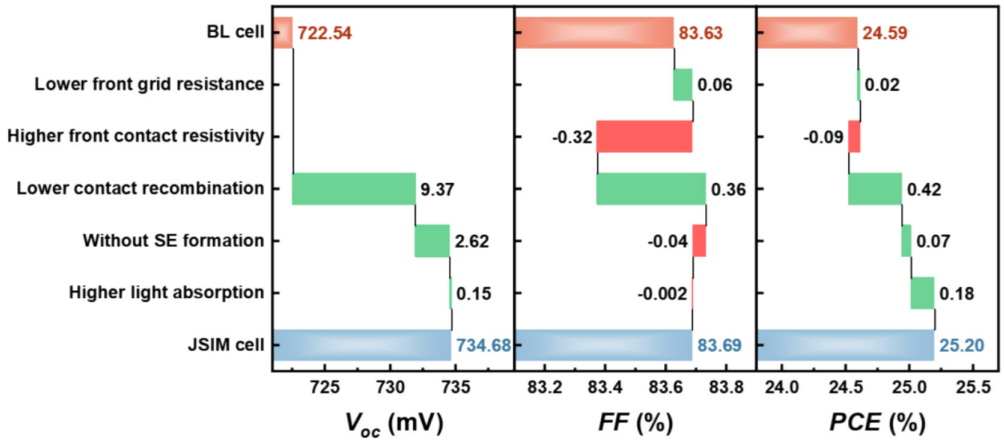

FIGURE 10 | Waterfall diagram showing the impact of the main differences between the baseline and JSIM TOPCon solar cells on the V_{oc}, *FF*, and *PCE*. The simulations were conducted in Quokka 3 and used the experimental values extracted in Sections 3.2–3.4.

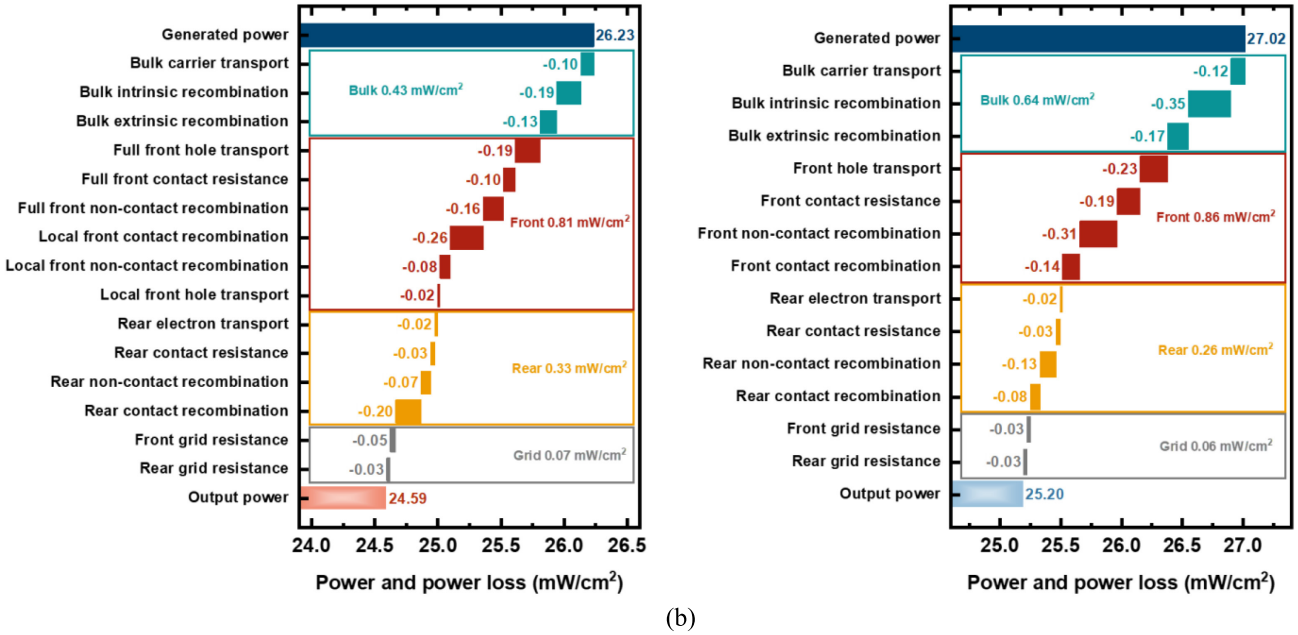

FIGURE 11 | Free energy loss analysis of (a) BL and (b) JSIM cells.

an effective method to improve the cell performance due to the reduced auger recombination. Improving the quality of Si bulk and surface passivation will also enhance the power output, as the bulk extrinsic recombination and front non-contact recombination caused electrical losses of ~0.17 mW/cm^2 and ~0.31 mW/cm^2, respectively. The front hole transport also led to ~0.23 mW/cm^2 loss, illustrating the necessity of carefully designing the sheet resistance when balancing the lateral transport, contact resistivity, contact recombination, light absorption, etc.

Considering that the JSIM cells still show the largest relative power loss due to the front side with a total of ~0.86 mW/cm^2, simulations regarding the optimization of the front side were conducted. According to Figure 12a, it is not surprising to see that lower contact resistivity and contact recombination can lead to higher *PCE*. If the front contact resistivity could be reduced to lower than 2 mΩcm^2, the cell efficiency would increase by ~0.1%$_{abs}$. Furthermore, a *PCE* of ~25.4% might be achieved if the optimized technology could decrease the contact resistivity and contact recombination to 1 mΩcm^2 and 40 fA/cm^2. Compared with the complexity of optimizing process parameters for recombination and resistive improvement, the modification of the screen-printing pattern is more straightforward. Figure 12b presents the simulated *PCE* with the variation of front-side finger contact width and contact pitch. Those two parameters were swept around the actual width (~24 μm) and pitch (~1 mm) of front contact, with the corresponding effects on shading, resistance, and recombination considered in the simulation. According to the simulated results, reducing the width of the front fingers clearly could increase the *PCE*, while the contact pitch showed a trade-off effect. Fortunately, with an optimized contact pitch (~0.7 mm), halving the finger width showed the potential of enhancing the *PCE* to ~25.5%,

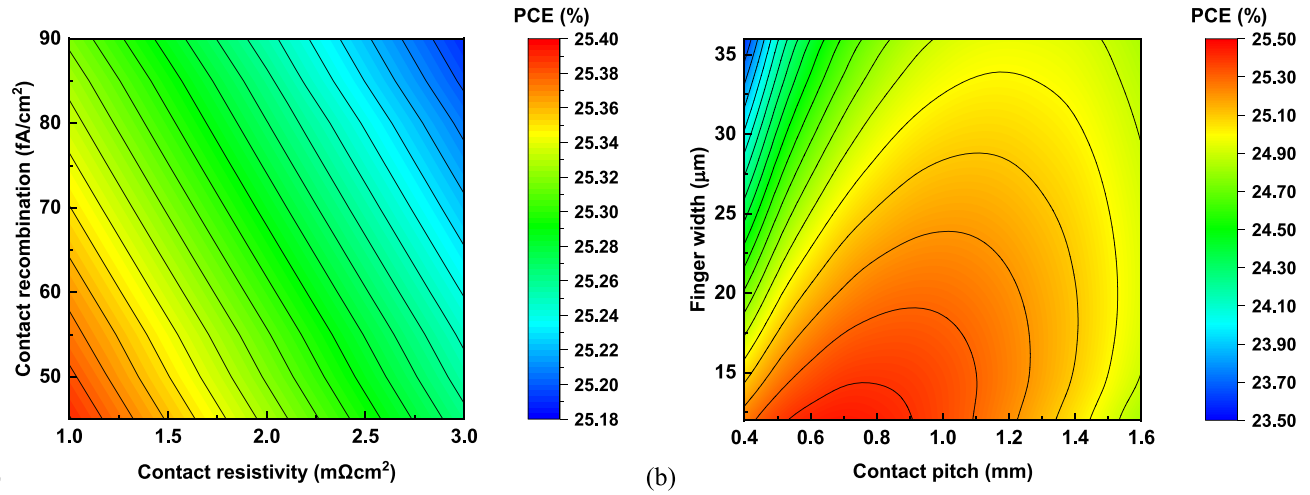

FIGURE 12 | Contour plot of JSIM cells with (a) the variation of front-side contact resistivity and contact recombination, and (b) the variation of front-side finger width and contact pitch.

which is even ~0.1%$_{abs}$ higher than the optimized case in Figure 12a. The results illustrate that re-designing the front gird pattern can also effectively improve the performance of JSIM cells further.

4 | Conclusion

Laser-assisted firing technology has been proven to improve the performance of TOPCon solar cells and thus garnered considerable interest in the industry in recent years. In this study, we evaluated the performance of TOPCon cells produced using the Jolywood Special Injected Metallization (JSIM) method, which is the laser-assisted firing process already used in the mass production line of Jolywood. This technique involves an additional laser scanning process combined with an applied reverse bias, after an initial co-firing step. The performance of JSIM cells was compared with baseline (BL) cells manufactured with conventional paste and a single-step firing process. Our findings demonstrated that laser-assisted firing significantly enhanced the performance of TOPCon solar cells, increasing the *PCE* by ~0.58%$_{abs}$. The front finger line resistance of JSIM cells was relatively lower due to the utilization of customized paste, but the front contact resistivity was higher which could be attributed to the lack of SE region. In terms of recombination losses, JSIM cells benefited from no SE laser doping process as well as lower front and rear contact recombination. Quokka 3 simulations confirmed that the reduction in contact recombination was the key factor driving the enhancement of *PCE*. Moreover, our electrical loss analysis indicated that front and rear contact recombination are no longer the dominant contributors to power loss in JSIM cells. To further enhance the cell performance, optimization of bulk resistivity and surface passivation quality could be beneficial. Additionally, the simulated results suggested that JSIM technology held the potential to further increase the *PCE* of high-volume produced TOPCon solar cells by ~0.3%$_{abs}$ with the optimized design of the front grid pattern. This study underscores the capability of laser-assisted firing to advance TOPCon solar cells toward their theoretical efficiency limits in large-scale production.

Acknowledgments

This work was supported by the Australian Government through the Australian Renewable Energy Agency (ARENA 1-60 Extension project) and the Australian Centre for Advanced Photovoltaics (ACAP), also funded by ARENA. The responsibility for the views, information, or advice expressed herein is not accepted by the Australian Government. The authors appreciate the support provided by the Australian Government's Trailblazer for Recycling & Clean Energy program, led by UNSW & the University of Newcastle. The authors express their gratitude to Dr. Yin Yao and Dr. Charlie Kong for their assistance and to the Electron Microscope Unit at The University of New South Wales (UNSW) for providing access to the ZEISS Cryogenic focused ion beam (Cryo-FIB) tool. Additionally, the authors appreciate the lifetime curve fitting code from Dr. Brendan Wright and the support from the UNSW LDOT team, both at the Solar Industrial Research Facility (SIRF) and the Tyree Energy Technologies Building (TETB). Xutao Wang acknowledges the University International Postgraduate Award (UIPA) Scholarship support from UNSW. Open access publishing facilitated by University of New South Wales, as part of the Wiley - University of New South Wales agreement via the Council of Australian University Librarians.

Conflicts of Interest

The authors declare no conflicts of interest.

Data Availability Statement

The data that support the findings of this study are available from the corresponding author upon reasonable request.

References

1. T. G. Allen, J. Bullock, X. Yang, A. Javey, and S. De Wolf, "Passivating Contacts for Crystalline Silicon Solar Cells," *Nature Energy* 4, no. 11 (2019): 914–928, https://doi.org/10.1038/s41560-019-0463-6.

2. F. Feldmann, M. Bivour, C. Reichel, M. Hermle, and S. W. Glunz, "Passivated Rear Contacts for High-Efficiency n-Type Si Solar Cells Providing High Interface Passivation Quality and Excellent Transport Characteristics," *Solar Energy Materials and Solar Cells* 120 (2014): 270–274, https://doi.org/10.1016/j.solmat.2013.09.017.

3. Z. Zhang, Y. Zeng, C. S. Jiang, et al., "Carrier Transport Through the Ultrathin Silicon-Oxide Layer in Tunnel Oxide Passivated Contact (TOPCon) c-Si Solar Cells," *Solar Energy Materials and Solar Cells* 187 (2018): 113–122, https://doi.org/10.1016/j.solmat.2018.07.025.

4. D. Chen, Y. Chen, Z. Wang, et al., "24.58% Total Area Efficiency of Screen-Printed, Large Area Industrial Silicon Solar Cells With the Tunnel Oxide Passivated Contacts (i-TOPCon) Design," *Solar Energy Materials and Solar Cells* 206 (2020): 110258, https://doi.org/10.1016/j.solmat.2019.110258.

5. F. Feldmann, M. Bivour, C. Reichel, H. Steinkemper, M. Hermle, and S. W. Glunz, "Tunnel Oxide Passivated Contacts as an Alternative to Partial Rear Contacts," *Solar Energy Materials and Solar Cells* 131 (2014): 46–50, https://doi.org/10.1016/j.solmat.2014.06.015.

6. F. Feldmann, C. Reichel, R. Müller, and M. Hermle, "The Application of Poly-Si/SiOx Contacts as Passivated top/Rear Contacts in Si Solar Cells," *Solar Energy Materials and Solar Cells* 159 (2017): 265–271, https://doi.org/10.1016/j.solmat.2016.09.015.

7. "EU/Trinasolar Announces Efficiency of 26.58% for Its n-Type TOPCon Cells, Setting a New World Record," Trina Solar, accessed December 09, 2024, https://static.trinasolar.com/eu-en/resources/newsroom/eu-trinasolar-announces-efficiency-2658-its-n-type-topcon-cells-setting-new-world.

8. "Trina Solar Claims Record-Breaking Efficiency of 26.58% for TOPCon Solar Cell", pv Magazine International. accessed December 09, 2024, https://www.pv-magazine.com/2024/11/21/trina-solar-claims-record-breaking-efficiency-of-26-58-for-topcon-solar-cell/.

9. B. Kafle, B. S. Goraya, S. Mack, F. Feldmann, S. Nold, and J. Rentsch, "TOPCon – Technology Options for Cost Efficient Industrial Manufacturing," *Solar Energy Materials and Solar Cells* 227 (2021): 111100, https://doi.org/10.1016/j.solmat.2021.111100.

10. ITRPV, *International Technology Roadmap for Photovoltaic* (VDMA, 2024).

11. Y. Chen, D. Chen, C. Liu, et al., "Mass Production of Industrial Tunnel Oxide Passivated Contacts (I-TOPCon) Silicon Solar Cells With Average Efficiency Over 23% and Modules Over 345 W," *Progress in Photovoltaics: Research and Applications* 27, no. 10 (2019): 827–834, https://doi.org/10.1002/pip.3180.

12. S. Ma, B. Liao, F. Y. Qiao, et al., "24.7% Industrial Tunnel Oxide Passivated Contact Solar Cells Prepared Through Tube PECVD Integrating With Plasma-Assisted Oxygen Oxidation and in-Situ Doped Polysilicon," *Solar Energy Materials and Solar Cells* 257 (2023): 112396, https://doi.org/10.1016/j.solmat.2023.112396.

13. R. Chen, M. Wright, D. Chen, et al., "24.58% Efficient Commercial n-Type Silicon Solar Cells With Hydrogenation," *Progress in Photovoltaics: Research and Applications* 29, no. 11 (2021): 1213–1218, https://doi.org/10.1002/pip.3464.

14. B. Liao, X. Wu, W. Wu, et al., "Tube-Type Plasma-Enhanced Atomic Layer Deposition of Aluminum Oxide: Enabling Record lab Performance for the Industry With Demonstrated Cell Efficiencies >24%," *Progress in Photovoltaics: Research and Applications* 31, no. 1 (2023): 52–61, https://doi.org/10.1002/pip.3607.

15. Y. Chen, D. Chen, P. P. Altermatt, et al., "Technology Evolution of the Photovoltaic Industry: Learning From History and Recent Progress," *Progress in Photovoltaics: Research and Applications* 31, no. 12 (2023): 1194–1204, https://doi.org/10.1002/pip.3626.

16. T. Gao, Q. Yang, X. Guo, et al., "An Industrially Viable TOPCon Structure With Both Ultra-Thin SiOx and n+−Poly-Si Processed by PECVD for p-Type c-Si Solar Cells," *Solar Energy Materials and Solar Cells* 200 (2019): 109926, https://doi.org/10.1016/j.solmat.2019.109926.

17. B. Liao, W. Wu, R. J. Yeo, et al., "Atomic Scale Controlled Tunnel Oxide Enabled by a Novel Industrial Tube-Based PEALD Technology With Demonstrated Commercial TOPCon Cell Efficiencies > 24%," *Progress in Photovoltaics: Research and Applications* 31, no. 3 (2023): 220–229, https://doi.org/10.1002/pip.3627.

18. I. Sánchez-Aniorte, R. Barrio, A. Casado, et al., "Optimization of Laser-Firing Processes for Silicon-Heterojunction Solar-Cell Back Contacts," *Applied Surface Science* 258, no. 23 (2012): 9443–9446, https://doi.org/10.1016/j.apsusc.2011.09.108.

19. P. Ortega, A. Orpella, I. Martín, et al., "Laser-Fired Contact Optimization in c-Si Solar Cells," *Progress in Photovoltaics: Research and Applications* 20, no. 2 (2012): 173–180, https://doi.org/10.1002/pip.1115.

20. D. Ourinson, G. Emanuel, K. Rahmanpour, et al., "Laser-Powered Co-Firing Process for Highly Efficient Si Solar Cells," *IEEE Journal of Photovoltaics* 11, no. 2 (2021): 282–288, https://doi.org/10.1109/JPHOTOV.2020.3043856.

21. T. Fellmeth, H. Höffler, S. Mack, et al., "Laser-Enhanced Contact Optimization on iTOPCon Solar Cells," *Progress in Photovoltaics: Research and Applications* 30, no. 12 (2022): 1393–1399, https://doi.org/10.1002/pip.3598.

22. E. Krassowski, S. Großer, M. Turek, A. Henning, and H. Zhao, "Investigation of Monocrystalline p-Type PERC Cells Featuring the Laser Enhanced Contact Optimization Process and new LECO Paste," *AIP Conference Proceedings* 2367, no. 1 (2021): 020005, https://doi.org/10.1063/5.0056380.

23. E. Krassowski, B. Jaeckel, M. Pander, D. Daßler, and S. Malik, "Assessing the Long-Term Stability of Laser Enhanced Contact Optimization (LECO) Treated PERC Cells in PV Modules by Extended Indoor and Outdoor Durability Tests," *EPJ Photovoltaics* 14 (2023): 13, https://doi.org/10.1051/epjpv/2023004.

24. E. Krassowski, T. Luka, V. Naumann, M. Turek, S. Großer, and H. Zhao, "Degradation Stability of Solar Cells After Laser Enhanced Contact Optimization (LECO)," *AIP Conference Proceedings* 2487, no. 1 (2022): 020009, https://doi.org/10.1063/5.0089704.

25. H. Zhao, 'Method for Improving the Ohmic Contact Behavior Between a Contact Grid and an Emitter Layer of a Silicon Solar Cell', August 15, 2019, accessed January 22, 2024, https://patentscope.wipo.int/search/en/detail.jsf?docId=WO2019154450.

26. E. Krassowski, B. Jaeckel, U. Zeller, et al., "Reliability Evaluation of Photovoltaic Modules Fabricated From Treated Solar Cells by Laser-Enhanced Contact Optimization Process," *Solar RRL* 6, no. 5 (2022): 2100537, https://doi.org/10.1002/solr.202100537.

27. H. Höffler, T. Fellmeth, F. Maischner, J. Greulich, E. Krassowski, and A. Henning, "Enlarged Firing Window and Efficiency Boosting of PERC Solar Cells by "Laser Enhanced Contact Optimization" (LECO)," *AIP Conference Proceedings* 2487, no. 1 (2022): 110001, https://doi.org/10.1063/5.0089264.

28. R. Mayberry, K. Myers, V. Chandrasekaran, A. Henning, H. Zhao and E. Hofmüller, "Laser Enhanced Contact Optimization (LECO) and LECO-Specific Pastes–A Novel Technology for Improved Cell Efficiency", in *36th European Photovoltaic Solar Energy Conference and Exhibition*, 2019.

29. S. Großer, E. Krassowski, S. Swatek, H. Zhao, and C. Hagendorf, "Microscale Contact Formation by Laser Enhanced Contact Optimization," *IEEE Journal of Photovoltaics* 12, no. 1 (2022): 26–30, https://doi.org/10.1109/JPHOTOV.2021.3129362.

30. Y.-B. Xie, C.-Y. Fang, D.-S. Chen, H. Yue, and S.-H. Huang, "Influence of Laser Induced Sintering on Contact of TOPCon Solar Cells," *Acta Physica Sinica* 73, no. 24 (2024): 248801, https://doi.org/10.7498/aps.73.20241372.

31. Y. Fan, S. Zou, Y. Zeng, et al., "Investigation of the Ag–Si Contact Characteristics of Boron Emitters for n-Tunnel Oxide-Passivated Contact Solar Cells Metallized by Laser-Assisted Current Injection Treatment," *Solar RRL* 8, no. 13 (2024): 2400268, https://doi.org/10.1002/solr.202400268.

32. Q. Wang, K. Guo, S. Gu, W. Huang, W. Wu, and J. Ding, "Investigation on Effects of the Laser-Enhanced Contact Optimization Process With Ag Paste in a Boron Emitter for n-TOPCon Solar Cell," *Progress in Photovoltaics: Research and Applications* 33, no. 2 (2025): 294–308, https://doi.org/10.1002/pip.3854.

33. R. Zhou, Y. Li, Z. Zhang, et al., "Nano-size Joule-Heating to Achieve Low-Ohmic Ag–Si Contact on Boron Emitters of n-TOPCon Solar Cells," *Small* 21, no. 4 (2025): 2409628, https://doi.org/10.1002/smll.202409628.

34. X. Wu, X. Wang, W. Yang, et al., "Enhancing the Reliability of TOPCon Technology by Laser-Enhanced Contact Firing," *Solar Energy Materials and Solar Cells* 271 (2024): 112846, https://doi.org/10.1016/j.solmat.2024.112846.

35. A. Mette, S. Hörnlein, F. Stenzel, et al., "Q.ANTUM NEO With LECO Exceeding 25.5% Cell Efficiency," *Solar Energy Materials and Solar Cells* 277 (2024): 113110, https://doi.org/10.1016/j.solmat.2024.113110.

36. A. Fell, J. Schön, M. C. Schubert, and S. W. Glunz, "The Concept of Skins for Silicon Solar Cell Modeling," *Solar Energy Materials and Solar Cells* 173 (2017): 128–133, https://doi.org/10.1016/j.solmat.2017.05.012.

37. H. Höffler, F. Simon, E. Krassowski, and J. Greulich, "Understanding Current Paths and Temperature Distributions During "Laser Enhanced Contact Optimization" (LECO)," *AIP Conference Proceedings* 2826, no. 1 (2023): 040002, https://doi.org/10.1063/5.0141008.

38. D. Inns and D. Poplavskyy, "Measurement of metal induced recombination in solar cells," in *2015 IEEE 42nd Photovoltaic Specialist Conference (PVSC)*, (2015), 1–4. https://doi.org/10.1109/PVSC.2015.7356056.

39. T. Fellmeth, A. Born, A. Kimmerle, F. Clement, D. Biro, and R. Preu, "Recombination at Metal-Emitter Interfaces of Front Contact Technologies for Highly Efficient Silicon Solar Cells," *Energy Procedia* 8 (2011): 115–121, https://doi.org/10.1016/j.egypro.2011.06.111.

40. D. Herrmann, S. Lohmüller, H. Höffler, A. Fell, A. A. Brand, and A. Wolf, "Numerical Simulations of Photoluminescence for the Precise Determination of Emitter Contact Recombination Parameters," *IEEE Journal of Photovoltaics* 9, no. 6 (2019): 1759–1767, https://doi.org/10.1109/JPHOTOV.2019.2938400.

41. S. Tepner and A. Lorenz, "Printing Technologies for Silicon Solar Cell Metallization: A Comprehensive Review," *Progress in Photovoltaics: Research and Applications* 31, no. 6 (2023): 557–590, https://doi.org/10.1002/pip.3674.

42. K.-K. Hong, S.-B. Cho, J. S. You, J.-W. Jeong, S.-M. Bea, and J.-Y. Huh, "Mechanism for the Formation of ag Crystallites in the ag Thick-Film Contacts of Crystalline Si Solar Cells," *Solar Energy Materials and Solar Cells* 93, no. 6 (2009): 898–904, https://doi.org/10.1016/j.solmat.2008.10.021.

43. J. D. Fields, M. I. Ahmad, V. L. Pool, et al., "The Formation Mechanism for Printed Silver-Contacts for Silicon Solar Cells," *Nature Communications* 7, no. 1 (2016): 11143, https://doi.org/10.1038/ncomms11143.

44. W. Wu, K. E. Roelofs, S. Subramoney, K. Lloyd, and L. Zhang, "Role of Aluminum in Silver Paste Contact to Boron-Doped Silicon Emitters," *AIP Advances* 7, no. 1 (2017): 015306, https://doi.org/10.1063/1.4974752.

45. X. Li, Q. Q. Wang, X. Dong, et al., "Optimization of Efficiency Enhancement of TOPCon Cells With Boron Selective Emitter," *Solar Energy Materials and Solar Cells* 263 (2023): 112585, https://doi.org/10.1016/j.solmat.2023.112585.

46. U. Jäger, S. Mack, C. Wufka, A. Wolf, D. Biro, and R. Preu, "Benefit of Selective Emitters for p-Type Silicon Solar Cells With Passivated Surfaces," *IEEE Journal of Photovoltaics* 3, no. 2 (2013): 621–627, https://doi.org/10.1109/JPHOTOV.2012.2230685.

47. D. Kray, N. Bay, G. Cimiotti *et al*., "Industrial LCP Selective Emitter Solar Cells With Plated Contacts", in *2010 35th IEEE Photovoltaic Specialists Conference*, June 2010, 000667–000671. https://doi.org/10.1109/PVSC.2010.5616896.

48. M. Kim, D. Kim, D. Kim, and Y. Kang, "Influence of Laser Damage on the Performance of Selective Emitter Solar Cell Fabricated Using Laser Doping Process," *Solar Energy Materials and Solar Cells* 132 (2015): 215–220, https://doi.org/10.1016/j.solmat.2014.08.021.

49. K. Ohmer, Y. Weng, J. R. Köhler, H. P. Strunk, and J. H. Werner, "Defect Formation in Silicon During Laser Doping," *IEEE Journal of Photovoltaics* 1, no. 2 (2011): 183–186, https://doi.org/10.1109/JPHOTOV.2011.2173298.

50. Z. Hameiri, T. Puzzer, L. Mai, A. B. Sproul, and S. R. Wenham, "Laser Induced Defects in Laser Doped Solar Cells," *Progress in Photovoltaics: Research and Applications* 19, no. 4 (2011): 391–405, https://doi.org/10.1002/pip.1043.

51. Q. Wang, S. Gu, K. Guo, H. Peng, W. Wu, and J. Ding, "Influence of the Medium-Temperature Light Soaking Process on the Passivation and Electronic Performance of the N-TOPCon Solar Cells," *Solar Energy Materials and Solar Cells* 273 (2024): 112959, https://doi.org/10.1016/j.solmat.2024.112959.

52. Q. Wang, H. Peng, S. Gu, et al., "High-Efficiency n-TOPCon Bifacial Solar Cells With Selective Poly-Si Based Passivating Contacts," *Solar Energy Materials and Solar Cells* 259 (2023): 112458, https://doi.org/10.1016/j.solmat.2023.112458.

53. P. Padhamnath, J. K. Buatis, A. Khanna, et al., "Characterization of Screen Printed and Fire-Through Contacts on LPCVD Based Passivating Contacts in monoPoly™ Solar Cells," *Solar Energy* 202 (2020): 73–79, https://doi.org/10.1016/j.solener.2020.03.087.

54. R. Brendel, S. Dreissigacker, N.-P. Harder, and P. P. Altermatt, "Theory of Analyzing Free Energy Losses in Solar Cells," *Applied Physics Letters* 93, no. 17 (2008): 173503, https://doi.org/10.1063/1.3006053.